1994ApJ...432..128P

THE ASTROPHYSICAL JOURNAL, 432:128–134, 1994 September 1
© 1994. The American Astronomical Society. All rights reserved. Printed in U.S.A.

GALAXY PROPERTIES IN DIFFERENT ENVIRONMENTS. II. STAR FORMATION IN BULGES OF LATE-TYPE SPIRALS

M. G. PASTORIZA,[1,2] E. BICA,[1] M. MAIA,[3] CH. BONATTO,[1,2] AND H. DOTTORI[1]
Received 1993 September 13; accepted 1994 February 25

ABSTRACT

The star formation history in the nucleus of late spiral galaxies is compared between a sample in a high galaxy density medium (HDS) and a control sample (CS) of isolated galaxies. We have observed 20 HDS and 18 CS galaxies from a larger list generated by the application of a group-finding algorithm to the SSRS survey. Using equivalent widths of absorption lines and the continuum distribution, we determined the nuclear stellar population types, from those dominated by old population to those containing star formation bursts of different ages and intensities. The HDS and CS stellar population type histograms are similar, suggesting that environmental influences, at least for the present sample, do not affect substantially the nuclear stellar population. However, the nuclear emission lines indicate that, in the BPT diagnostic diagrams, there is an excess of HDS galaxies located within or close to the AGN loci. For six HDS and two CS galaxies, it was possible to determine oxygen (O/H) and nitrogen (N/H) abundances. The samples present similar O/H values, but in the CS galaxies the N/O ratio is lower at equal galaxy luminosity.

Subject headings: galaxies: abundances — galaxies: spiral — galaxies: stellar content — stars: formation

1. INTRODUCTION

The influence of the local density of galaxies on their star formation rate (SFR) is not yet well understood. Two effects have been suggested to influence the SFR in spiral galaxies in high-density regions. On the one hand, the SFR could be enhanced by tidal interactions (Bushouse 1986; Kennicutt et al. 1987). On the other hand, close galaxy encounters may lead to a depletion of interstellar gas and thus produce preferentially anemic spirals in cluster galaxies. Galaxies located within superclusters live in an environment significantly denser than that experienced by isolated galaxies, but close encounters are still not frequent enough to strip the gas as in the case of galaxies in clusters (Maia & da Costa 1990). In the latter work it was also found that the Hα equivalent width of galaxies in groups tends to be larger than those outside, which could be interpreted as enhanced star formation in galaxies in groups. A comparison between cluster and field spirals suggested that Hα emission seems to be dependent on the morphological type (Moss & Whittle 1993).

A detailed analysis of the absorption- and emission-line spectra could help to clarify the dependence of the SFR on the galaxy environment starburst contributions larger than 1% in mass relative to the old stellar population should produce detectable spectroscopic features (Bica, Alloin, & Schmidt 1990). Otherwise recent star formation events as well as nuclear activity can be traced by the emission lines of the ionized gas, and information on the gas chemical and physical properties can be derived from photoionization models.

The aim of this work is to study the various stellar components and the emitting gas seen globally through an aperture corresponding to the central 1.2 kpc for a high density (HDS) and a low density control (CS) samples of galaxies, which were generated in Maia et al. (1994, hereafter Paper I). The sample properties are described in § 2, and the observations, in § 3. The absorption-line spectrum analysis is performed in § 4, where we determine the stellar population types and compare their characteristics in the two samples. In § 5 we subtract stellar population templates in order to carry out a pure emission-line spectrum analysis. We use diagnostic diagrams to classify the emission-line spectra, and for the galaxies with the strongest lines we derive gas physical parameters as well as oxygen and nitrogen abundances. We summarize our conclusions in § 6.

2. THE SAMPLES

The SSRS catalog (da Costa et al. 1988, 1989, 1991) was taken as a database for the selection of the two samples. The selection procedure used to generate the samples is described in detail in Paper I. Basically a group-finding algorithm (Maia, da Costa, & Latham 1989) was applied to the SSRS catalog to select the galaxies for the HDS and CS samples. The CS corresponds to galaxies, according to the search procedure, which turn out to be nonmembers of groups. The lower density cutoff for the HDS is 18 galaxies Mpc^{-3}, and the upper one for the CS is 0.0004 galaxies Mpc^{-3}. All morphological types were included in that analysis.

In the present paper we discuss the results for a subsample of the late spirals (Sb to Sc) which are brighter than $B \approx 14.0$ mag. In addition we have avoided edge-on galaxies, since our spectral analysis deals with the central regions. The final HDS and CS galaxies are listed in Tables 1A and 1B respectively, where the morphological type, visual magnitude, axial ratio, and foreground reddening are from Lauberts & Valentijn (1989). The radial velocity is from the SSRS. We also provide foreground reddening-corrected absolute magnitudes calculated with those data.

3. OBSERVATIONS

The spectrophotometric observations were collected in 1991 August and 1992 July/November with the 1 m telescope of the Cerro Tololo Inter-American Observatory using the

[1] Departmento de Astronomia, IF-UFRGS, CP 15051, CEP91501-970, Porto Alegre, RS, Brazil.
[2] Visiting Astronomer at the Cerro Tololo Inter-American Observatory, operated by the Association of Universities for Research in Astronomy, Inc. under contract with the National Science Foundation.
[3] Departmento de Astronomia, Observatório Nacional, Rua Gal. José Cristino 77, Rio de Janerio, Rio de Janerio, 20921-RJ, Brazil.

© American Astronomical Society • Provided by the NASA Astrophysics Data System

1994ApJ...432..128P

TABLE 1A

FUNDAMENTAL DATA FOR THE HDS

ESO	Galaxy	T	b/a	B	A_B	V_R	M_{B_0}
0352053....	NGC 491	3	0.73	13.30	0.16	3577	−19.5
3530060....	NGC 574	2	0.71	14.20	0.00	5445	−19.5
2970060....	NGC 626	5.5	0.92	13.40	0.00	5287	−20.2
1530170....	...	5	0.79	13.90	0.02	6172	−20.1
5450110....	NGC 908	5	0.48	11.00	0.00	1202	−19.4
5460150....	NGC 1099	3	0.35	14.00	0.04	7314	−20.3
3570190....	NGC 1310	5	0.77	13.00	0.02	1408	−17.7
5480310....	NGC 1353	3	0.41	12.00	0.03	1266	−18.5
3580170....	NGC 1365	3	0.71	10.10	0.00	1289	−20.5
5480710....	NGC 1414	3.8	0.19	14.65	0.04	1241	−15.8
3580580....	NGC 1437	3	0.69	12.50	0.00	785	−17.0
1180430....	NGC 1672	4	0.89	10.50	0.00	989	−19.5
1190060....	NGC 1688	7.5	0.47	12.57	0.00	876	−17.1
3050060....	NGC 1792	3.4	0.50	10.70	0.04	876	−19.0
2330410....	NGC 6870	2	0.53	13.20	0.14	2442	−18,7
1080130....	NGC 7179	3.5	0.37	13.80	0.01	2669	−18.7
4060270....	NGC 7418A	7	0.90	13.85	0.00	1806	−17.4
2910120....	NGC 7552	2.5	0.89	11.20	0.00	1316	−19.4
2910160....	NGC 7582	1	0.37	10.90	0.00	1304	−19.7
2400130....	...	3	0.69	14.10	0.00	2938	−18.2

TABLE 1B

FUNDAMENTAL DATA FOR THE CS

ESO	Galaxy	T	b/a	B	A_B	V_R	M_{B_0}
3500140....	NGC 101	6	1.00	13.40	0.00	3111	−19.1
5410010....	...	3.5	0.62	14.00	0.05	6042	−19.9
5430120....	...	3	0.47	...	0.00	4715	...
4780280....	NGC 922	9	0.65	12.54	0.00	2769	−19.7
1150280....	NGC 1096	4	1.00	13.70	0.06	6106	−20.2
5480750....	...	5	1.00	14.00	0.18	6866	−20.2
4840250....	NGC 1591	12	0.67	13.80	0.04	3806	−19.1
4220120....	IC 2106	4	0.54	13.80	0.00	4638	−19.5
1420500....	IC 4901	5	0.67	12.30	0.13	1920	−19.1
2870460....	...	6	0.63	14.30	0.00	4578	−19.0
1890070....	NGC 7141	4	0.67	12.70	0.07	2725	−19.5
1450220....	IC 5141	4.5	0.78	13.50	0.05	4212	−19.6
6010190....	...	6	0.35	15.00	0.06	7030	−19.2
4050180....	NGC 7267	1	0.83	12.97	0.08	3137	−19.5
5330450....	...	3	0.92	13.40	0.02	5580	−20.3
5340110....	NGC 7341	1.3	0.42	13.30	0.04	4191	−19.8
5350150....	...	6	0.48	...	0.05	5839	...
6050070....	IC 5321	3	0.62	14.00	0.06	2676	−18.1
4720100....	...	4.5	0.44	14.70	0.03	3735	−18.2

Cassegrain spectrograph and 2D-Frutti two-dimensional photon-counting detector. The galaxies were observed with a slit width of 5″. The spectral region covered was $\lambda\lambda$3600–7000, with a 5 Å resolution at λ5000. All spectra were flux calibrated using standard stars from Stone & Baldwin (1983). The extracted spectra, integrated along the slit length correspond in each galaxy to 1.2 kpc. They have been corrected by Galactic absorption using A_B values from Lauberts & Valentijn (1989), and for the galaxies without such values, we have interpolated values from neighboring ones in Burstein & Heiles (1984).

4. THE ABSORPTION-LINE SPECTRA

The stellar population analysis for the galaxy samples are based on the equivalent widths (W) of the absorption features listed in Table 2A and Table 2B. The continuum tracing and the spectral windows are those defined by Bica & Alloin (1986a). Typical errors are $\sigma \approx 0.5$ Å.

These W values were used to classify each galaxy in terms of Bica's (1988) templates, which span the properties of the more usual nuclear stellar populations observed in normal galaxies. The basic characteristics of the groups can be summarized as follows: S1–S3 are red stellar population with metallicity decreasing from ≈4 to 1 times solar. The S4–S7 is a sequence of increasing contribution of blue components such that S4 contains ≈10% flux contribution at 5870 Å of population younger than 1 Gyr and S7 contains ≈70%. Most galaxies of the HDS and CS match these templates (see Tables 2A and 2B). We illustrate the template match for a blue and a red population case in Figure 1. One galaxy of the HDS matches the template E7 which has a significant contribution of an intermediate age component. For a few cases it was necessary to slightly modify the templates with inclusion of an excess H II region continuum; these cases are indicated with a plus sign attached to the template type.

The internal reddening of each galaxy, affecting the nuclear stellar population mostly due to inclination effects, was estimated following Bica & Alloin (1986b). After determining the stellar population template by means of the W values (excluding Na I), in some cases the corresponding template was bluer than that of the observed galaxy. Matching the continua with a normal reddening law, it was possible to estimate the internal reddening $E(B-V)_i$ which is listed in Tables 2A and 2B.

The frequency of the stellar population types of the galaxies of the HDS and CS sample, illustrated in the histograms (Fig. 2) do not show remarkable differences. This indicates that there is not a clear relation between the frequency of stellar

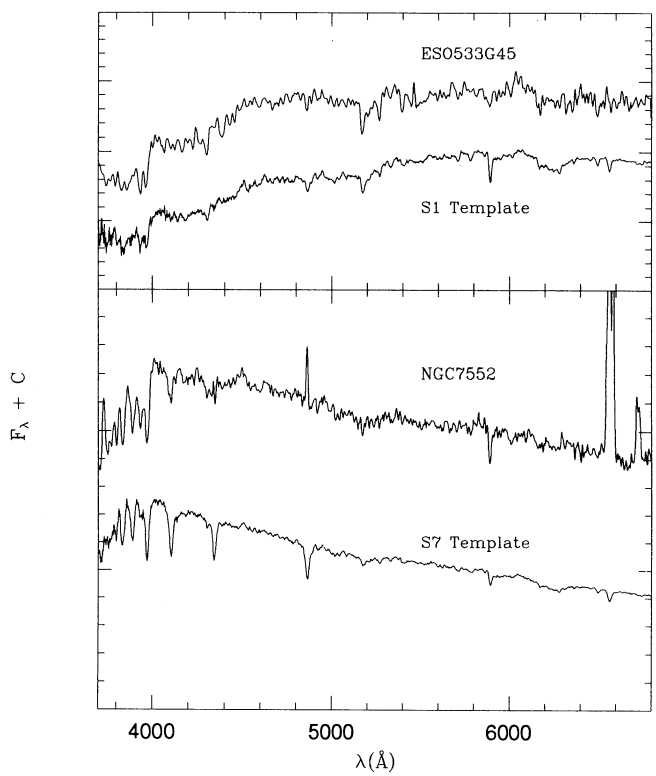

FIG. 1.—Examples of stellar population types in the sample and corresponding templates. *Upper panel*: a red metal-rich case with foreground $E(B-V)_i = 0.00$. *Lower panel*: a blue case, where $E(B-V)_i = 0.20$ was applied to fit the template; notice the interstellar Na I λ5890 excess relative to the template. The spectra are normalized to $F_\lambda = 1$ at 5870 Å, with additive constant for visualisation.

© American Astronomical Society • Provided by the NASA Astrophysics Data System

1994ApJ...432..128P

TABLE 2A

EQUIVALENT WIDTHS FOR THE HIGH-DENSITY SAMPLE

Name	Ca II	H	Hδ	CN	G	Hγ	Hβ	MgH	Mg I + MgH	MgH	Na I	Hα	Template	$E(B-V)_i$
NGC 491	15.6	11.9	2.8	7.1	6.2	3.1	1.8	2.7	7.2	4.7	3.2	11.3	S5	0.00
NGC 574	6.0	8.9	5.4	5.8:	2.4:	1.4:	−8.3	2.2	4.3	3.4	3.8	−92.5	S6	0.00
NGC 626	16.0	12.3	3.6	9.4	9.4	5.4	4.2	3.0	7.9	4.1	4.8	−1.4	S2	0.00
E153G17	12.9	11.1	4.1	4.3	6.5	3.8	2.9:	2.5:	6.7:	4.9:	...	3.6:	E7	0.00
NGC 908	15.9	12.7	6.0	6.9	7.3	4.2	2.9	4.5	7.7	6.2	5.2:	−5.4:	S3	0.10
NGC 1099	12.4	10.7	8.9:	10.7:	6.9:	4.5	3.2	6.2	12.2	7.2	7.1	−16.8	S4	0.00
NGC 1310	12.9	12.1	8.2	6.2	4.2	6.3	2.5	1.6	4.2	2.6	2.2	−16.6	S6+	0.00
NGC 1353	17.2	14.0	3.8	8.1	8.3	5.1	1.8	2.2	6.6	3.5	4.0	−7.0	S3	0.00
NGC 1365	8.0	7.5	2.3	3.3	4.4	1.0	−6.8	3.1	4.9	3.7	6.4	−106.	S5	0.00
NGC 1414	13.3	10.6	8.2:	...	9.6:	7.1:	...	...	...	...	...	−11.5	S6	0.00
NGC 1437	16.0	13.3	3.1:	5.9:	9.3	7.3	1.0:	1.4:	5.9	4.1:	...	−0.8	S4	0.00
NGC 1672	8.1	8.9	4.1	2.6	4.5	2.2	−1.8	2.4	4.7	2.8	4.6	−58.4	S6+	0.00
NGC 1688	6.9	10.2	5.3	5.2	4.4	4.8	−5.1	0.2	1.1	1.5	2.2:	−63.2	S7−	0.00
NGC 1792	11.4	10.4	4.6	3.3	6.8	4.3	0.9	1.1	3.8	2.8	2.8	−23.9	S5	0.05
NGC 6870	18.8	14.3	2.7	12.3	10.1	3.9	1.8	3.9	9.9	7.6	5.7	5.4	S1	0.00
NGC 7191	19.9	13.1	1.5:	7.7:	11.2	5.4	2.0:	5.3	10.2	6.1	5.9:	−0.9:	S1	0.00
NGC 7418A	8.7	4.8	−0.8	4.0:	6.6	−5.0	−17.2	1.5:	3.7:	4.6:	4.9	−89.3	S7	0.05
NGC 7552	6.7	8.5	4.3	2.7	3.3	4.1	−2.4	1.9	3.5	2.7	4.8	−91.8	S7	0.20
NGC 7582	10.9	8.7	2.9	5.1	4.9	0.5	−8.8	1.6	4.5	1.9	4.3	−106.	S5	0.10
E240G13	9.5	8.0	1.3	7.0	6.7	−1.9	−9.3	1.4	3.1	4.3	0.8:	−99.1	S5	0.05

TABLE 2B

EQUIVALENT WIDTHS FOR THE CONTROL SAMPLE

Name	Ca II	H	Hδ	CN	G	Hγ	Hβ	MgH	Mg I + MgH	MgH	Na I	Hα	Template	$E(B-V)_i$
NGC 101	9.0	8.1	3.4	2.7	7.0	2.2	1.5	1.3:	3.0:	3.2:	5.0:	−7.5:	S5	0.00
E541G1	18.2	14.1	4.7:	11.1:	10.7	5.9	4.4	3.3	10.9	6.8	5.6	2.9:	S1	0.00
R543G12	12.1	10.4	4.8	6.4:	4.5	3.3	4.9:	2.9:	8.7	6.7:	4.2	0.9:	S4	0.00
NGC 922	3.2	5.7	3.9	3.8	3.1	0.1	−13.3	0.1:	2.4	3.2:	2.4:	−118.0	S7+	0.00
NGC 1096	14.6	13.5	6.4:	...	7.2	6.1:	1.9:	2.9:	10.3	9.2:	6.5	−7.0	S3	0.05
E548G75	16.4	12.0	2.2	10.7	8.3	7.1	2.2	4.7	10.6	6.3	6.2	...	S3	0.00
NGC 1591	6.6	8.7	6.0	2.1:	4.6	1.8:	3.0	1.8:	4.7:	5.9:	3.5	−25.5	S6	0.00
IC 2106	5.9	8.6	4.3	6.4	6.4	2.3	2.4:	2.7	7.7	5.6	...	−11.8	S5	0.05
IC 4901	16.8	12.4	0.5	5.6	9.9	3.0	3.1:	2.6	6.8	5.0	4.1:	3.4:	S3	0.00
E287G46	9.9	6.5:	...	6.5:	7.5	...	...	...	6.8:	...	6.3:	−14.6	S6	0.00
NGC 7141	8.0	6.7	5.6	5.4	6.2	1.7	−1.8	2.8	5.8	3.0	6.3	−29.9	S6	0.15
IC 5141	14.9	14.0	5.8	6.1	6.4	3.5	4.1	3.4:	7.2	7.4:	...	−0.4:	S3	0.00
E601G19	8.9	10.6	6.3:	...	3.9:	...	4.9:	3.5:	7.1:	5.2:	...	−6.9:	S5	0.00
NGC 7267	6.8	7.2	6.4	4.0:	4.4	1.7	0.5	2.4	6.2	1.9	4.8	−27.0	S6	0.00
E533G45	18.8	15.1	6.6	12.7	9.5	4.7	3.1	2.7	10.2	7.4	3.1	−1.4	S1	0.00
NGC 7341	19.6	14.0	5.7	14.0	11.3	5.7	3.0	3.6	10.8	7.5	4.1	−1.1	S1	0.00
E535G15	10.5	10.3	6.7	4.4:	6.0	6.0	0.6:	2.6:	2.5:	3.3:	...	−26.7	S6	0.00
IC 5321	5.1	6.6	5.0	2.6:	4.7	3.3	−7.0	...	1.6:	3.1	2.5	−58.1	S7	0.00
E472G1	13.8	10.5	5.7:	...	8.9	8.0	2.9:	...	4.1:	...	...	−15.5	S5	0.00

population bursts in the bulges and the local density of galaxies, at least for the present galaxy sample. Taken at face value, the HDS histogram shows a small excess of blue galaxies S6 and S7, but larger samples would be necessary to check this result.

We have compared the behavior of the more prominent absorption features, which are sensitive to age and metallicity effects (Bica & Alloin 1987). Figures 3*a* through 3*c* show W versus W plots among the metallic features Ca II K, G band, (Mg I + MgH), and Na I. It is interesting to note that the range in the W values for the HDS and CS galaxies is essentially the same. This result suggests that the age and metallicity distributions of stellar components in the bulges of spiral galaxies do not depend much on the environment. However the plot W(Hα) versus W(Ca II K) (Fig. 4) shows that for the same range in the W(Ca II K), equivalent widths of Hα *in emission* larger than 50 Å are more frequently observed for the HDS galaxies. This result can be interpreted in terms of the frequency of star formation events in the two samples. Formation events must be so frequent in the HDS galaxies that most of the sample is currently forming stars, probably owing to a higher rate of galaxy interactions. As these bursts evolve and fade, they produce an accumulation of aged blue stellar populations. Nevertheless, the properties of these accumulations do not differ much from those arising from the less frequent bursts in the CS galaxies, since the stellar population types occurring in the two samples do not differ much (Fig. 2).

5. EMISSION LINES AND NUCLEAR ACTIVITY

We have subtracted the stellar population contribution from the calibrated spectra normalized at λ5870, using the templates from Bica (1988), according to the population types from Tables 2A and 2B. We verified that the underlying absorption does not much affect the Hα emission line, but it is very important for Hβ, especially when the emission and the absorption components have comparable intensities (see also Bonatto, Bica, & Alloin 1989). In Figure 5 we show examples of the pure emission-line spectra, shifted by arbitrary amounts: for a low-

© American Astronomical Society • Provided by the NASA Astrophysics Data System

1994ApJ...432..128P

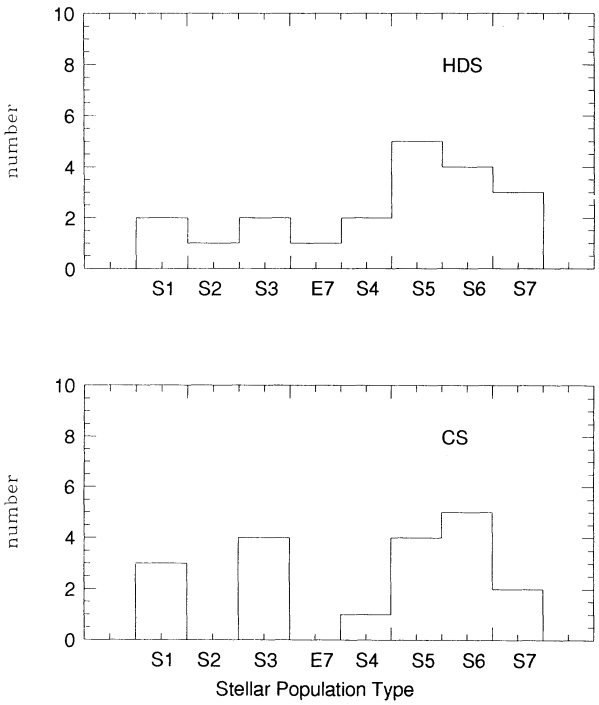

FIG. 2.—Histogram of stellar population types for the samples: S1–S3 are late-type stellar population with decreasing metallicity; E7 has an important intermediate-age component; S4–S7 have increasing contribution of young components.

luminosity LINER (NGC 574), two starburst nuclei (NGC 922 and NGC 7418A) and two Seyfert 2 nuclei (ESO 240G13 and NGC 7582). This illustrates the nuclear activity types observed in the galaxy samples. We have measured the fluxes by fitting Gaussians to the emission-line profiles. This procedure allowed us to deblend close lines. In the fittings we constrained the theoretical ratios [O III] λ4959 = 0.333 [O III] λ5007, and [N II] λ6548 = 0.333 [N II] λ6584. The resulting emission-line fluxes are listed in Tables 3A and 3B, respectively for the HDS and CS galaxies. The gas internal reddening values $E(B-V)_I$ are also shown, which have been estimated from the observed flux ratio $F(\mathrm{H}\alpha)/F(\mathrm{H}\beta)$ assuming a case B recombination value.

Usually, diagnostic diagrams with emission-line ratios of easily observed lines are employed to classify the spectra of extragalactic objects according to the main excitation mechanisms (Veilleux & Osterbrock 1987; Baldwin, Phillips, & Terlevich 1981). Figure 6 shows the diagnostic diagram [O III] λ5007/Hβ versus [N II] λ6583/Hα. In this figure, the area delimited by the solid line is occupied by Seyfert 2 narrow-line radio galaxies (NLRG) and LINERs, objects photoionized by a power-law continuum; the short-dashed curve encloses H II regions, nuclear H II regions, and starburst galaxies, objects photoionized by hot stars. Most of the HDS galaxies (*filled circles*) are located in the region occupied by the active galaxies or in the transition between an H II region and AGN, while the CS galaxies have H II region emission-line spectrum. The influence of the environment on the nuclear activity of the galaxies appears to occur. In fact Dahari (1984) found that more than 40% of AGN galaxies are interacting or close interacting

TABLE 3A

EMISSION-LINE FLUXES FOR THE HDS GALAXIES

Galaxy	[O II] λ3727	Hγ	Hβ	[O III] λ4959	[O III] λ5007	[N II] λ6548	Hα	[N II] λ6584	[S II] λ6717	[S II] λ6730	$E(B-V)_I$
NGC 491	...	...	...	...	...	13	100	40	...	...	...
NGC 574	18	...	35	...	...	17	100	53	26	2.4	0.35
NGC 1099	...	...	...	...	...	28	100	80	100	...	...
NGC 1310	203	...	...	...	...	2.0	100	60	...	...	...
NGC 1365	17.0	9.4	32	13	43	11	100	33	2.9	2.9	1.1
NGC 1414	48	...	...	...	...	...	100	...	...	...	...
NGC 1672	38	...	35	...	7.3	14	100	49	...	...	0.7
NGC 1688	66	12	35	2.5	7.4	7.7	100	24	...	...	0.1
NGC 1792	...	...	...	...	...	10	100	33	11	9.1	...
NGC 7418A	75	21	36	28	101	5.0	100	17	8.9	6.4	0.0
NGC 7552	31	20	34	...	...	4.1	100	54	11	9.4	0.61
NGC 7582	26	13	35	26	77	17	100	57	17	20	0.76
E240G13	31	21	35	5.2	14	19	100	38	7.9	7.6	0.61

TABLE 3B

EMISSION-LINE FLUXES FOR THE CS GALAXIES

Galaxy	[O II] λ3727	Hγ	Hβ	[O III] λ4959	[O III] λ5007	[N II] λ6548	Hα	[N II] λ6584	[S II] λ6717	[S II] λ6730	$E(B-V)_I$
NGC 922	73	14	35	8.2	25	6.0	100	19	18	18	0.00
NGC 1096	...	...	...	...	...	22	100	73	...	...	...
NGC 1591	83	...	35	...	...	...	100	23	...	...	0.69
IC 2106	...	...	...	...	...	...	100	...	...	...	...
NGC 7141	17	22	34	...	...	7.8	100	44	...	...	0.50
NGC 7267	16	22	35	...	...	14	100	46	...	...	0.50
E535G15	...	...	35	...	...	...	100	26	...	...	0.73
IC 5321	105	11	34	15	51	5.0	100	17	15	15	0.00

© American Astronomical Society • Provided by the NASA Astrophysics Data System

1994ApJ...432..128P

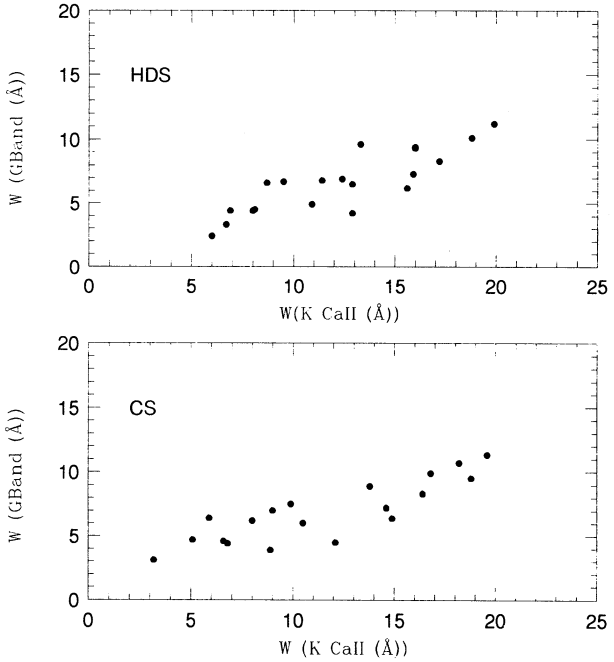

FIG. 3a

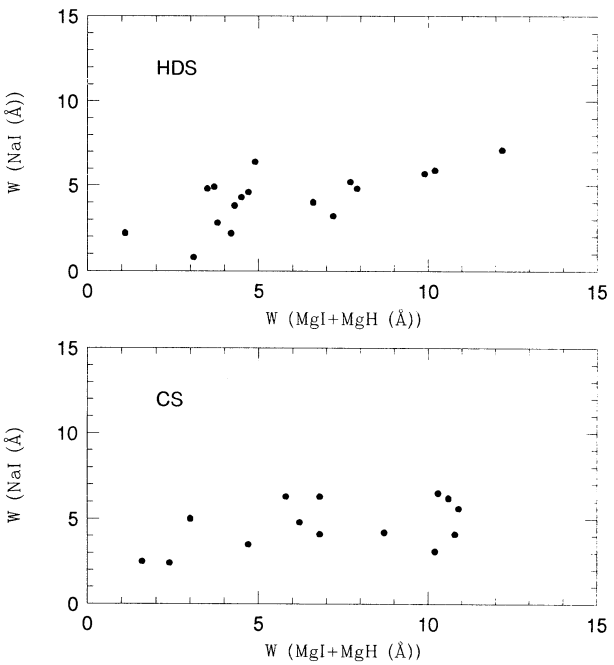

FIG. 3c

FIG. 3.—Comparison of equivalent widths of strong metallic absorption features for both samples: (*a*) G-band vs. K Ca II; (*b*) Mg I + MgH vs. Ca II K; (*c*) Na I vs. Mg I + MgH. Note the similar behavior for the two samples.

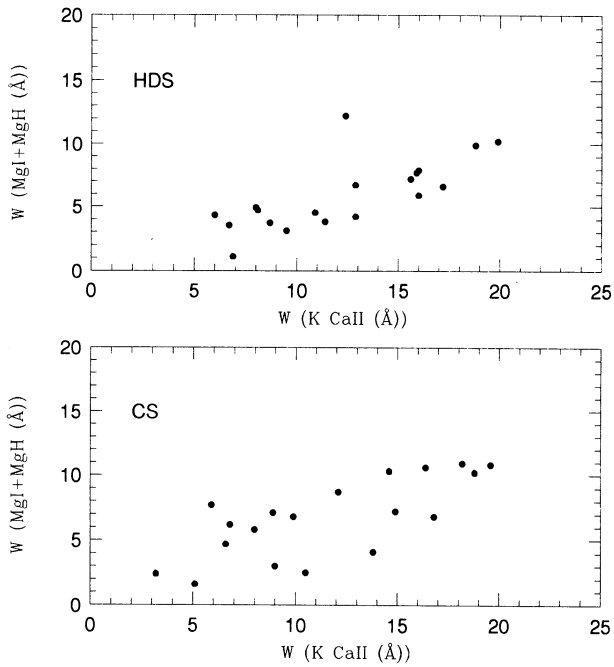

FIG. 3b

systems. We have also found by analysing the properties of the complete HDS and CS set (Paper I) that galaxies in high density environment present a larger fraction of Seyferts, as well as of barred galaxies.

6. GAS, OXYGEN, AND NITROGEN ABUNDANCES

Gas densities derived from the [S II] $\lambda\lambda$6717, 6731 line ratios, are listed in Table 4. The electronic temperature has been derived using the calibration of the [O III] λ5007 + 4959/[N II] λ6584 ratio against the mean electronic temperature (T[O III]) from a model sequence (Dopita & Evans 1986). The T[O III] values are listed in Table 4. The ionic and total abundances of O and N were calculated from their corresponding line intensity ratios and adopted electronic temperature following a three-level atom calculation using the atomic parameters given by Mendoza (1983). We assumed that the total abundances of O and N are given by the following: $O/H = O^+/H^+ + O^{++}/H^+$ and $N/H = N^+/H^+$. In Table 4 are listed the derived values of 12 + log (O/H) and log (N/O) for six HDS and two CS galaxies of our samples. In the case of NGC 7552 the [O III] lines are not detected in our spectra, so we have adopted the O and N abundances from Diaz (1985) derived from smaller aperture observation.

Of particular interest to the comparison of cluster and field spirals is the possibility of continuous accretion of primordial gas onto the disk of the field spirals (Gunn 1982). The chemical implications of the infall include a decrease in O/H at fixed

TABLE 4

CHEMICAL ABUNDANCES

Galaxy	T_e	N_e	12+log (O/H)	log (N/O)
E240G13	6100	450	8.48	−0.70
NGC 1365	7000	571	8.40	−0.82
NGC 1672	5628	500	8.66	−0.86
NGC 1688	6100	460	8.70	−1.10
NGC 7418A	7800	500	8.60	−1.40
NGC 7582	7000	570	8.60	−0.80
IC 5321	7000	400	8.68	−1.45
NGC 922	7000	300	8.59	−1.25
NGC 7552	...	...	8.95	−0.74
LMC	...	...	8.58	−1.58
NGC 4303	...	...	9.42	−0.87
NGC 3310	...	...	9.00	−1.63
M51	...	...	9.22	−0.78
M81	...	...	8.70	−0.85

© American Astronomical Society • Provided by the NASA Astrophysics Data System

1994ApJ...432..128P

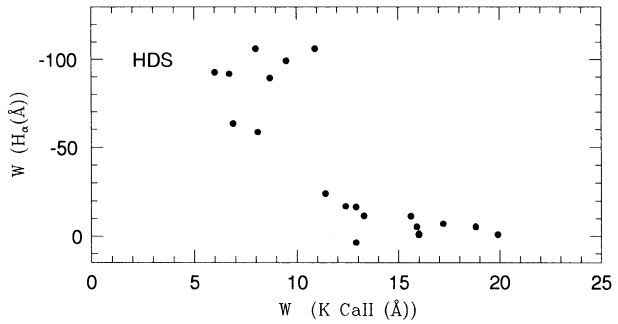

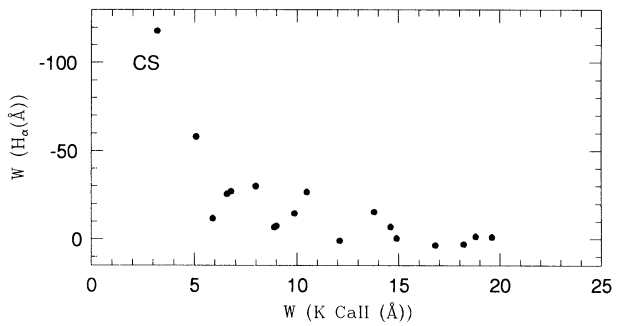

FIG. 4a

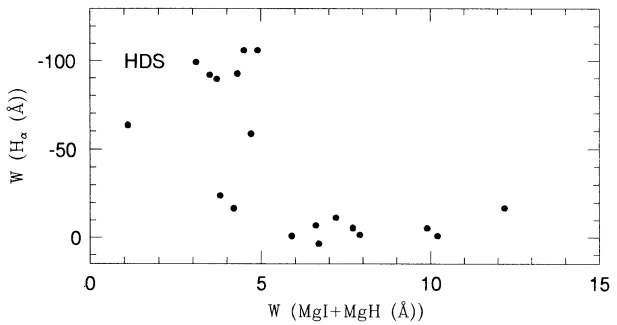

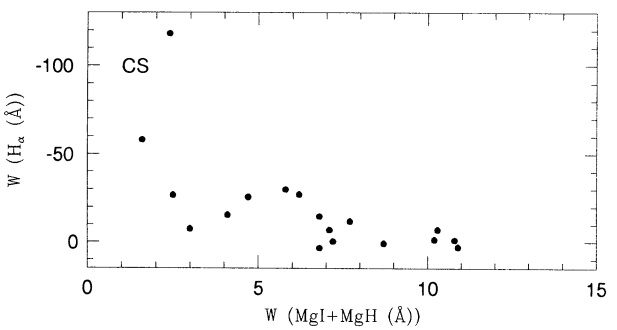

FIG. 4b

FIG. 4.—For the two samples, comparison of equivalent widths of Hα with a metallic feature (*a*) in the blue and (*b*) in the yellow. A difference is detected between the samples.

mass fraction ($N_{\rm H\,I}/M_T$) (Tinsley 1981) and a reduction in O/H for a given value of N/O (Serrano & Peimbert 1981). Evidence that spiral galaxies in the Virgo Cluster have systematically higher interestellar abundances than those of field galaxies has been presented by Shields, Skillman, & Kennicutt (1991). However, Henry et al. (1992) found that Virgo spirals and field galaxies are indistinguishable in terms of their abundance properties. In order to address this contradictory question we have made a comparison of our results for the HDS and CS galaxies with those for the Virgo spiral NGC 4303 (Henry et al. 1992), the well-known field spirals M51 (Diaz et al. 1991), and M81 (Garnett & Shields 1987) and the lower metallicity gal-

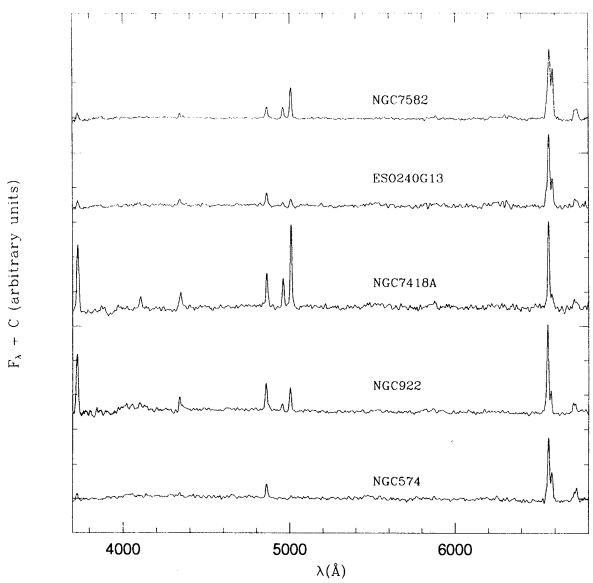

FIG. 5.—Examples of population-subtracted emission-line spectra in the samples. *Top to bottom*: Seyfert 2; Seyfert 2/H II region transition; excited H II region; lower excitation H II region; LINER.

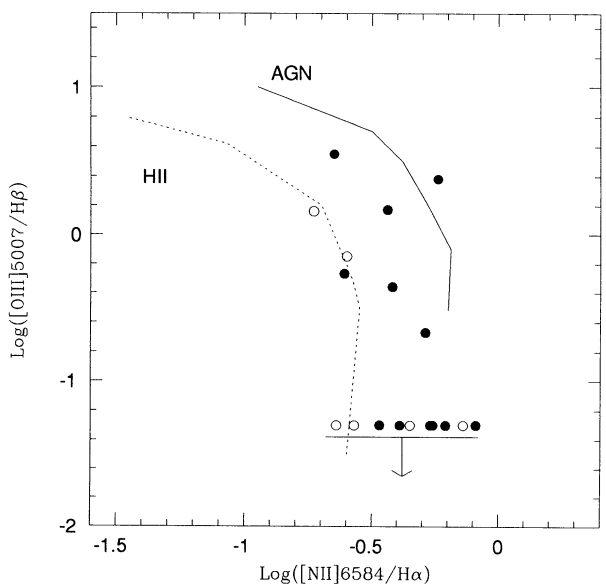

FIG. 6.—For galaxies with strong emission lines in the two samples, emission type diagnostic diagram where models for AGN and H II regions are plotted.

© American Astronomical Society • Provided by the NASA Astrophysics Data System

1994ApJ...432..128P

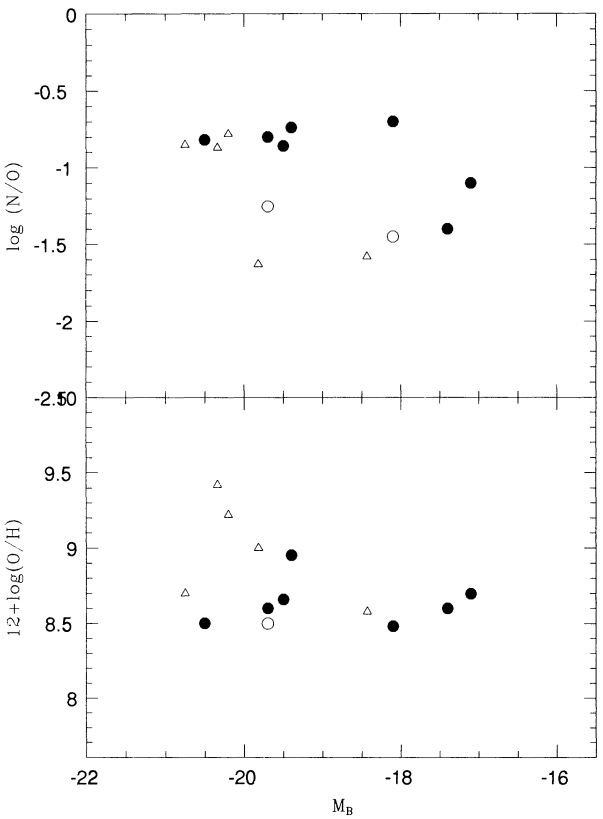

FIG. 7.—Comparison of 12 + log (O/H) and log (N/O) of HDS (*filled circles*), CS (*open circles*), and galaxies with M51, M81, NGC 4303, NGC 3310, and LMC (*triangles*).

axies NGC 3310 (Pastoriza et al. 1993) and the LMC (Torres-Peimbert, Peimbert, & Fierro 1989), as listed in Table 4. In Figure 7 are plotted log (N/O) and 12 + log (O/H) versus the absolute magnitude M_{B_0}. In the O/H diagram, the HDS and the CS galaxies present similar values, independently of galaxy luminosity, a result in agreement with that of Henry et al. (1992). On the other hand in the N/O diagram there is some correlation between N/O and absolute magnitude for the HDS galaxies; for equal luminosity, the CS galaxies present lower N/O than those in the HDS. The CS O/H and N/O values are comparable to those of the LMC. These findings suggest that environment does not have much effect on oxygen abundances but may play some role with nitrogen. In fact as most of the HDS galaxies in Figure 7 are AGNs or transition objects, the N variations may be related to nuclear activity (Storchi-Bergmann & Pastoriza 1989).

7. CONCLUSIONS

We have compared the stellar populations and the gas emission properties between a sample in a high galaxy density medium and a control sample of isolated galaxies. We used equivalent widths of absorption lines and the continuum distribution to determine the nuclear stellar population types, whose histograms are similar in the two samples, suggesting that environmental influences do not affect substantially these populations. Emission-line diagnostic diagrams indicate an excess of HDS galaxies located within or close to the AGN locus. The galaxies in the samples with strong emission lines allowed us to determine oxygen and nitrogen abundances. The samples present similar O/H values, but the isolated galaxies show lower N/O than those in a high galaxy density medium at equal galaxy luminosity.

REFERENCES

Baldwin, J. A., Phillips, M. M., & Terlevich, R. 1981, PASP, 93, 5
Bica, E. 1988, A&A, 195, 76
Bica, E., & Alloin, D. 1986a, A&A, 162, 21
———. 1986b, A&A, 166, 83
———. 1987, A&AS, 70, 281
Bica, E., Alloin, D., & Schmidt, A. 1990, MNRAS, 242, 241
Bonatto, Ch., Bica, E., & Alloin, D. 1989, A&A, 226, 23
Burstein, D., & Heiles, C. 1984, ApJS, 54, 33
Bushouse, H. A. 1986, AJ, 91, 225
da Costa, L. N., Pellegrini, P. S., Davis, M., Meiksin, A., Sargent, W. L. W., & Tonry, J. 1991, ApJS, 75, 935
da Costa, L. N., et al. 1988, ApJ, 327, 544
da Costa, L. N., Pellegrini, P. S., Willmer, C., de Carvalho, R., Maia, M. A. G., Latham, D. W., & Geary, J. C. 1989, AJ, 97, 315
Dahari, O. 1984, AJ, 89, 966
Diaz, A. 1985, Ph.D. thesis, Univ. of Sussex, Brighton
Diaz, A., Terlevich, E., Vilchez, J., Pagel, B., & Edmunds, M. G. 1991, MNRAS, 253, 245
Dopita, M. A., & Evans, I. A. 1986, ApJ, 307, 431
Garnett, D. R., & Shields, G. A. 1987, ApJ, 82, 101
Gunn, J. E. 1982, in Astrophysical Cosmology, ed. H. A. Bruck, G. V. Coyne, & M. S. Longair (Vatican City: Pontifica Academia Scientarum), 233
Henry, R. B. C., Pagel, B., Lasseter, D. F., & Chincarini, G. 1992, MNRAS, 258, 231
Kennicutt, R. C., Keel, W. C., van der Hulst, J. M., Hummel, E., & Roettinger, K. A. 1987, AJ, 93, 1011
Lauberts, A., & Valentijn, E. A. 1989, The Surface Photometry Catalogue of the ESO-Uppsala Galaxies (Garching bei München: ESO)
Maia, M. A. G., & da Costa, L. N. 1990, ApJ, 352, 457
Maia, M. A. G., da Costa, L. N., & Latham, D. W. 1989, ApJS, 69, 809
Maia, M. A. G., Pastoriza, M. G., Bica, E., & Dottori, H. 1994, ApJS, 93, 425 (Paper I)
Mendoza, C. 1983, in IAU Symp. 103, Planetary Nebulae, ed. D. R. Flower (Dordrecht: Reidel), 143
Moss, C., & Whittle, M. 1993, ApJ, 407, L17
Pastoriza, M. G., Dottori, H., Terlevich, E., Terlevich, R., & Diaz, A. 1993, MNRAS, 260, 177
Serrano, A., & Peimbert, M. 1989, Rev. Mexicana Astron. Af., 8, 117
Shields, G., Skillman, E. D., & Kennicutt, R., Jr. 1991, ApJ, 371, 82
Stone, R. P. S., & Baldwin, J. A. 1983, MNRAS, 204, 357
Storchi-Bergmann, T., & Pastoriza, M. G. 1989, ApJ, 347, 195
Torres-Peimbert, S., Peimbert, M., & Fierro, J. 1989, ApJ, 345, 186
Tinsley, B. M. 1981, ApJ, 250, 758
Veilleux, S., & Osterbrock, D. E. 1987, ApJS, 63, 295

© American Astronomical Society • Provided by the NASA Astrophysics Data System